01 Jan 1973

Individual Realization Laser-Doppler Technique Applied to Turbulent Channel Flow

W. G. Tiederman

D. K. McLaughlin

M. M. Reischman

INDIVIDUAL REALIZATION LASER DOPPLER TECHNIQUE APPLIED TO TURBULENT CHANNEL FLOW

W. G. Tiederman, D. K. McLaughlin, and M. M. Reischman
School of Mechanical and Aerospace Engineering
Oklahoma State University
Stillwater, Oklahoma 74074

ABSTRACT

Measurements of the mean and turbulence intensity of the streamwise velocity component in a fully developed, two-dimensional channel flow of water are presented. The measurements were made with the individual realization laser Doppler technique and emphasize the near-wall region of the flow. A dual-scatter optical arrangement was used which employs 90^{o} scattering and yields a probe volume whose length normal to the wall is 0.0075 inches. A correction has been made to the data that accounts for the statistical biasing which occurs in the individual realization technique. The corrected data demonstrate that the individual realization technique can yield accurate velocity estimates in the near-wall region where turbulent fluctuations are large.

INTRODUCTION

For several years a group at Oklahoma State University has been interested in making laser Doppler velocity measurements in fully developed, two-dimensional, turbulent channel flows of liquids. The original motivation was to use these measurements to determine the wall shear stress and thereby deduce the amount of drag reduction in the flow of a dilute polymer solution whose near-wall region was being visualized. A description of the individual realization technique used to make these laser anemometer measurements and the results in water flows were presented by Donohue, McLaughlin and Tiederman (2). A limited number of measurements in drag-reducing flows appear in Donohue, Tiederman, and Reischman (3); however, this original channel and technique were not suitable for making extremely accurate velocity measurements in the near-wall region of a drag-reducing flow, and that is our present goal. Therefore, a new channel and a new laser Doppler anemometer were developed. Moreover, the accurate utilization of individual realization turbulence data requires that a correction (See McLaughlin and Tiederman (9)), be applied to the data when the velocity fluctuations are large. The purpose of this paper is to describe our current individual realization anemometer technique (including the implementation of the correction) and to present results for turbulent channel flows of water. These measurements verify the "standard" character of the channel, and show that the individual realization technique will yield accurate results even in regions of high turbulent fluctuations.

INDIVIDUAL REALIZATION TECHNIQUE AND BIASING CORRECTION

The essential points about an individual realization laser amenometer are that the signal is not continuous and that velocity realizations occur only when a scattering center is in the probe volume. The appearance of a scatter center

in the probe volume is a random event with the probability of the event occurring being proportional to the volume of fluid swept through the probe volume. If a number of these realizations are recorded in a histogram, the experimenter may calculate the mean and the root mean square of the fluctuation by systematically taking moments of the distribution of individual realizations.

Unfortunately, the mean velocity calculated from the histogram, $\overline{U}_b$, given by

$$\overline{U}_b = \frac{1}{N} \sum_{i=1}^{N} U_i \qquad (1)$$

is greater than the time-average velocity $\overline{U}_t$ calculated from

$$\overline{U}_t = \frac{1}{T} \int_{t}^{t+T} U(t)dt \quad , \qquad (2)$$

because the ensemble of data making up the histograms are biased to the high velocity side. The biasing occurs because a larger than average volume of fluid, and hence a larger than average number of scattering centers pass through the probe volume during periods when the velocity is faster than the mean. Similarly a smaller volume of fluid and a smaller number of scattering particles pass through the probe volume during periods when the velocity is slower than the mean. This is easily seen in Figure 1 where the area under any segment of the velocity trace is proportional to the volume flow through the probe volume. Figure 2 also shows how a typical probability density distribution of the axial velocity component is biased. An important feature of the biasing is that the spread of the distribution is changed very little, instead the whole curve is shifted to higher velocities. Because of this feature, Reference 9 demonstrates that estimates of the root mean square of the fluctuation component of the velocity are best made from the original biased distributions.

Correction to the mean velocity estimates must be made, however, when the level of turbulence intensity is above about 15%. In fact, for a root mean square fluctuation level of 30%, the mean estimate must be corrected by 8%.

The correct method for calculating the time-average velocity from the histogram of individual realizations is to weight each velocity realization with the inverse of the absolute magnitude of the velocity vector. In this case, the corrected mean estimate is

$$\overline{U} = \frac{\sum_{i=1}^{N} \omega_i U_i}{\sum_{i=1}^{N} \omega_i} \quad , \qquad (3)$$

where the true weighting functions are

$$\omega_i = \frac{1}{|\vec{V}_i| \gamma_i} \quad . \qquad (4)$$

However, there are two simple ways to make the biasing correction on the mean estimate. The first and most direct approach is to use one-dimensional weighting functions in place of the true three-dimensional ones where the one-dimensional (approximate) weighting functions are

$$\omega_i = \frac{1}{U_i} \qquad (5)$$

A substantial simplification results when the one-dimensional weighting functions are substituted into Equation 3, namely

$$\overline{U} = \frac{N}{\sum_{i=1}^{N} \frac{1}{U_i}} \qquad (6)$$

Equation 6 may be rewritten as

$$\overline{U} = \left(\frac{\lambda}{2 \sin \theta/2}\right) / \overline{T}_D \qquad (7)$$

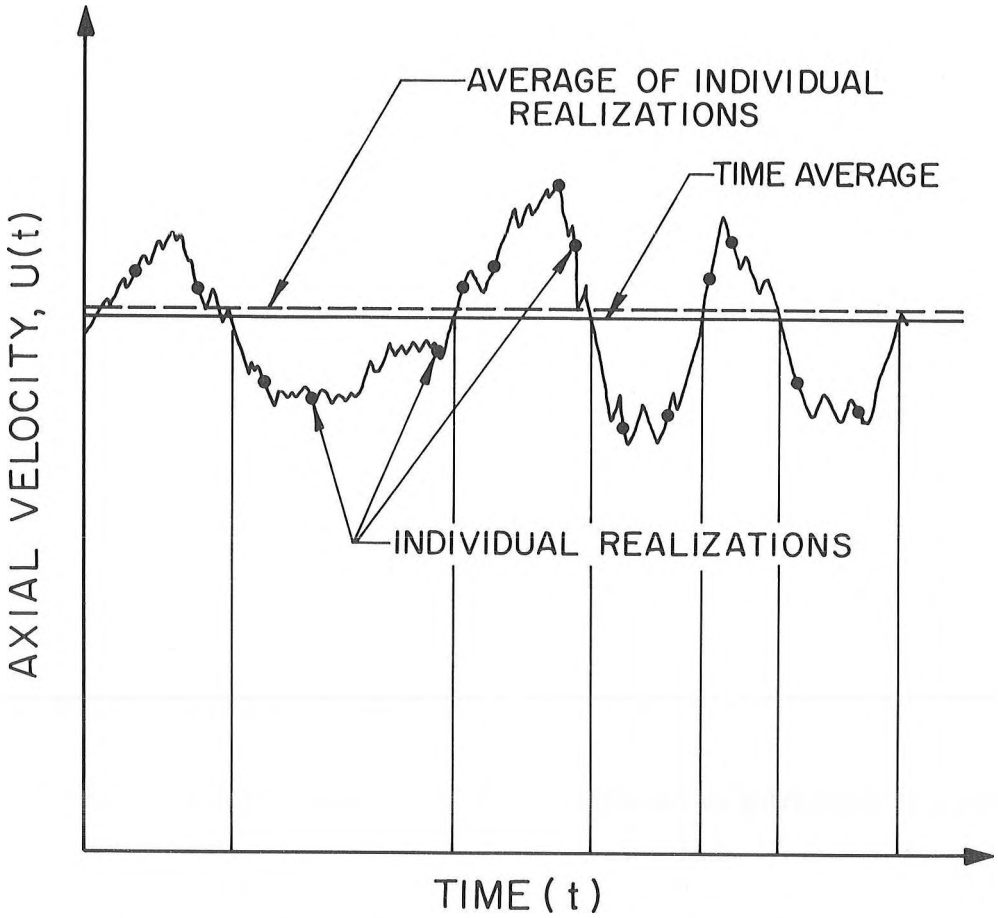

Figure 1. Comparison of Time-Average and Individual Realization Mean Velocities for Turbulent Flow

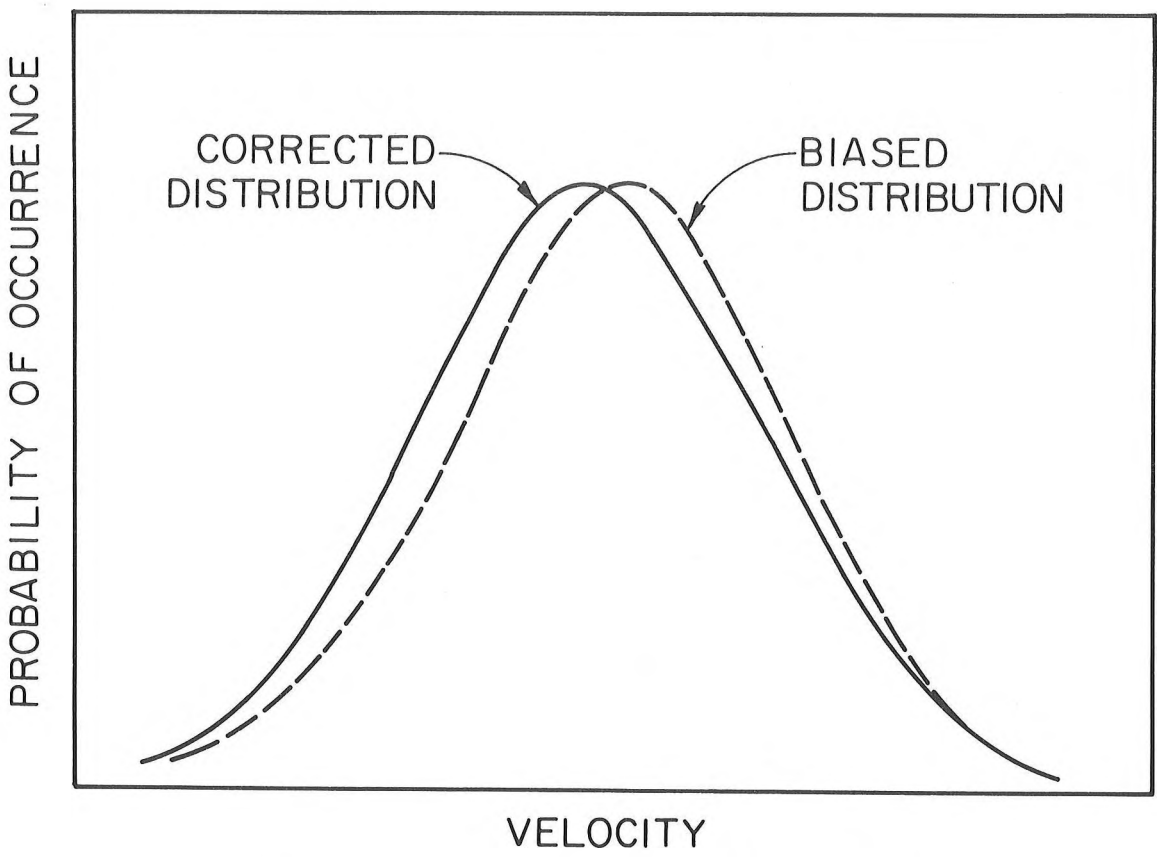

Figure 2. Comparison of Biased and Corrected Velocity Histograms

where $\overline{T}_D$ is the average Doppler period for N realizations. Since the Doppler period may be measured directly, this is an efficient approach for implementing the one-dimensional biasing correction with experimental data.

The second method of correcting for the natural bias is to use the curves generated in McLaughlin and Tiederman (9). These correction curves have been calculated using two-dimensional weighting functions and turbulent flow models based upon Gaussian-like probability density distributions.

Besides the natural histogram biasing, a correction is also needed to account for significant velocity gradients across the probe volume. The basic principal involved in the velocity gradient correction is the same as in the biasing correction, namely, at the outer locations within the probe volume there is on the average a larger volume flow and a larger number of particles passing through that portion of the probe volume. Karpuk (8) has demonstrated that the estimate of the time-average velocity given by Equation 6 yields the time-average velocity for a finite probe volume in which there is a significant mean velocity gradient. If the mean velocity gradient is linear, then the time-average velocity for the finite width is the same as the time-average velocity at the geometric center of the probe volume. Since the spatial resolution is critical only in the near-wall region where the mean velocity gradient is linear, it is sufficient to assume that the estimate given by Equation 6 is the time average velocity at the geometric center of the probe volume.

A finite mean velocity gradient across the probe volume will also affect the measured estimate of the root mean square of the velocity fluctuation, u'. In particular, the measured value will be larger than the value of u' at a point. This problem becomes increasingly severe as the wall is approached. However, for the majority of the data here, the effect should be small; and no correction has been applied to account for the difficulty.

TEST APPARATUS AND PROCEDURE

The channel and the anemometer were designed to maximize the spatial resolution in the near-wall region of the channel by making the probe volume as small as possible, particularly in the direction normal to the wall. A schematic of the basic optical system which is a dual-scatter or fringe anemometer system, is shown in Figure 3. The system uses a Spectra Physics model 130, 5 mw helium-neon laser and a RCA model 7326 photo-multiplier tube. Since the intersecting light beams from the laser form an ellipsoidal volume, improved spatial resolution was achieved by orienting the channel and the optics so that the long dimension of the ellipsoid is parallel to the wall and the minimum dimension is normal to the channel wall. It is important to note that only light scattered from the intersection of the beams will have the Doppler frequency.

As shown in Figure 3, the photomultiplier tube receives light which is scattered at a 90^o angle from the plane of the intersecting incident beams. The intensity of the scattered light is close to a minimum at this angle. However, the arrangement has three advantages. The laser, photomultipler tube and optics are all mounted on a single, mechanically simple, traversing mechanism. Further there is very little optical noise which reaches the photomultiplier tube because the intersection of the incident beams with the channel walls is outside the view of the receiving optics. And finally, the 90^o orientation gives the experimenter the ability to minimize the long dimension of the probe volume by focusing the collecting optics on only part of the ellipsoid of intersection.

In water, the angle between the intersecting laser beams, θ, is 5.59 degrees, and the beams are focused to a $1/e^2$ diameter of 0.0099 inches at their intersection. However, the effective diameter of the probe volume is smaller than this because there must be 10 cycles of the Doppler signal above the trigger level of the data-processing electronics. Observation of the maximum number of Doppler cycles present for typical trigger levels yields an estimated probe volume diameter of

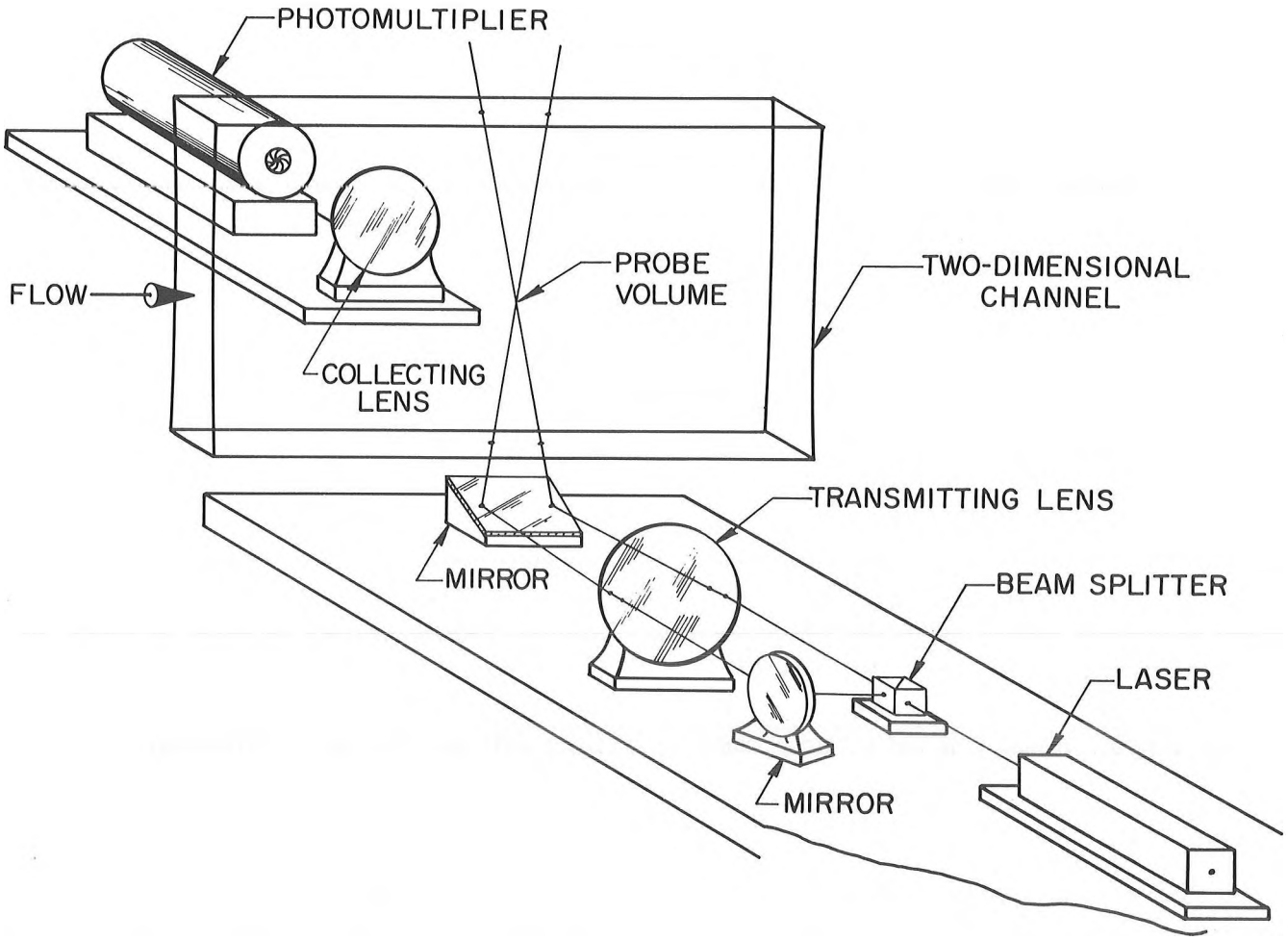

Figure 3. Side-Scatter Individual Realization Laser Doppler Anemometer

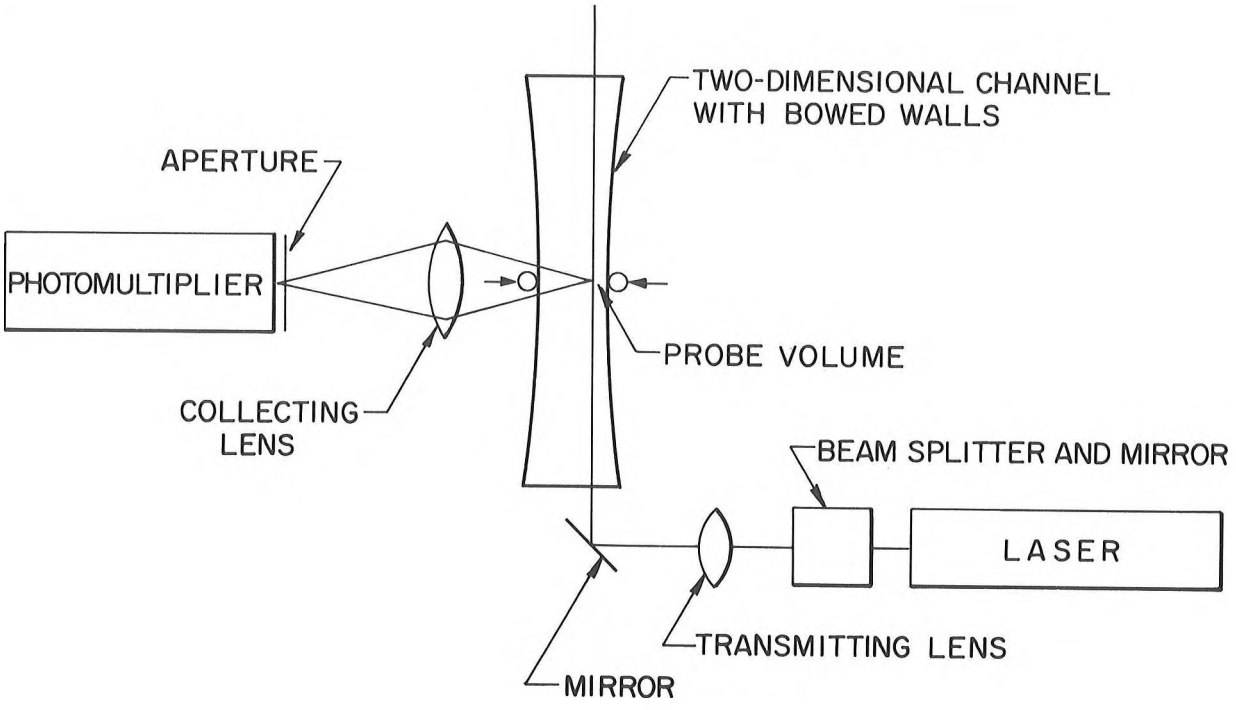

Figure 4. Schematic of Flow Channel and Optical Components

0.0075 inches. Due to the collecting lens and the aperture, the only focused light reaching the photomultiplier tube comes from the center 0.025 inches of the ellipsoid formed by the intersection of the two incident beams. Therefore, the probe volume is essentially a cylinder with a diameter of 0.0075 inches and a length of 0.025 inches, the long dimension being parallel to the wall.

In order to fully utilize the optical arrangement, the clear plastic channel walls are each bowed inward 0.045 inches along the entire length so that the probe volume can be traversed up to either wall without interference (see Figure 4). All of the optical components are rigidly mounted on a single traversing mechanism which allows the probe volume to be moved completely across the channel and to be positioned with an accuracy of $\pm$0.0005 inches. The measurement station is 54 inches downstream of a sharp-edged entrance; the channel width, W, is 1.020 inches at the center, and the channel is 12 inches high.

The major function of the data acquisition electronics is to measure the Doppler period of an individual realization generated from the light scattered from a single particle passing through the probe volume. The presence of stray pulses and noise on the Doppler signals means that the validity of each realization whose Doppler period is being counted must be established to insure that 10 consecutive Doppler cycles from a single realization have been measured. A digital logic system which will verify individual realization signals is currently being developed, but in the meantime, each signal is verified visually. This verification is accomplished by first processing each bandpass filtered wave packet with a Schmitt trigger. The Schmitt trigger transforms each cycle of the Doppler burst which has an amplitude above the trigger setting into a pulse. Thus, the Schmitt trigger output is a constant amplitude pulse train and the occurrence of a missing or an extraneous pulse is immediately obvious. Its output simultaneously triggers a storage oscilloscope and a General Radio model 1192B digital counter which is operating in the "period times ten" mode. When the operator visually verifies a realization on the oscilloscope, the counter reading is recorded and processed later by digital computer. The verification specifically consists of a visual inspection of any signal which triggers the counter to make certain that it contains 10 successive Doppler cycles above the trigger level. It is not uncommon for either stray pulses to trigger the counter or for Doppler bursts to contain one or two cycles in the middle of the packet with amplitudes below the trigger level. Either situation yields a time which is not the period for 10 cycles from a single realization and these counts must be rejected.

An important ingredient in the data acquisition and reduction system shown schematically in Figure 5 is the tape recorder. All photo-detector signals are recorded on an Ampex model 1300 tape recorder using a 60 inch/sec. tape speed. The tape is played back during data reduction at 7-1/2 inches/sec. This time expansion gives a human operator time to make decisions about the validity of each realization while the tape is being played back. The permanent record is also useful for repetitive data reduction to help evaluate the uncertainty in the measurement technique.

There are about 40 usable fringes in the probe volume. This number is sufficient so that the lower limit of a band pass filter can be set between the Doppler frequencies and the pedestal frequencies which are inversely proportional to the particle transit time through the probe volume. This filter setting must be done carefully in turbulent flows with high fluctuation levels. As illustrated in Figure 6, the gap between the lowest Doppler frequency and the highest pedestal frequency can become too small if one has an insufficient number of fringes in the probe volume and a high level of fluctuation. This is a fundamental limitation when the velocity is near zero in the probe volume because it then becomes impossible

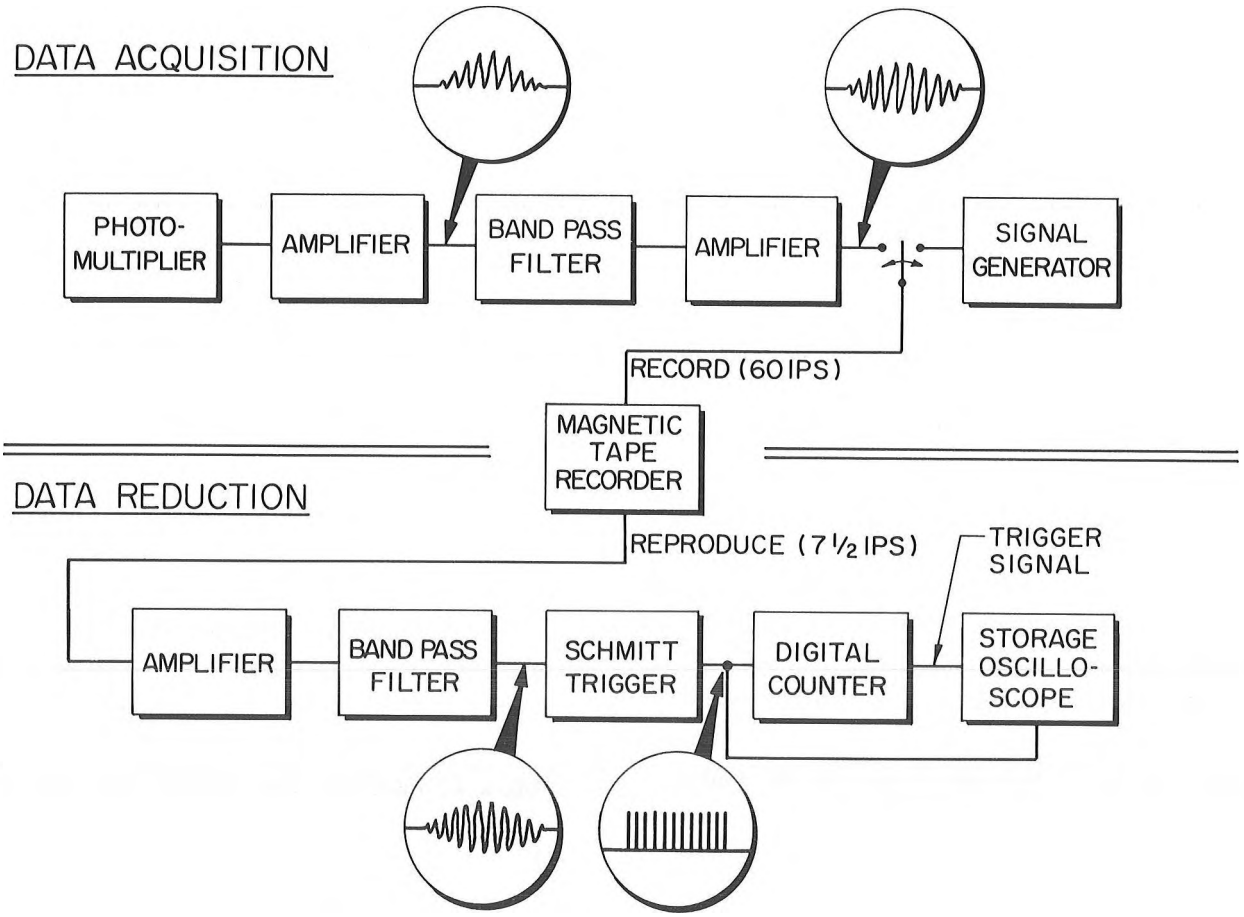

Figure 5. Block Diagram of Data Acquisition and Reduction System

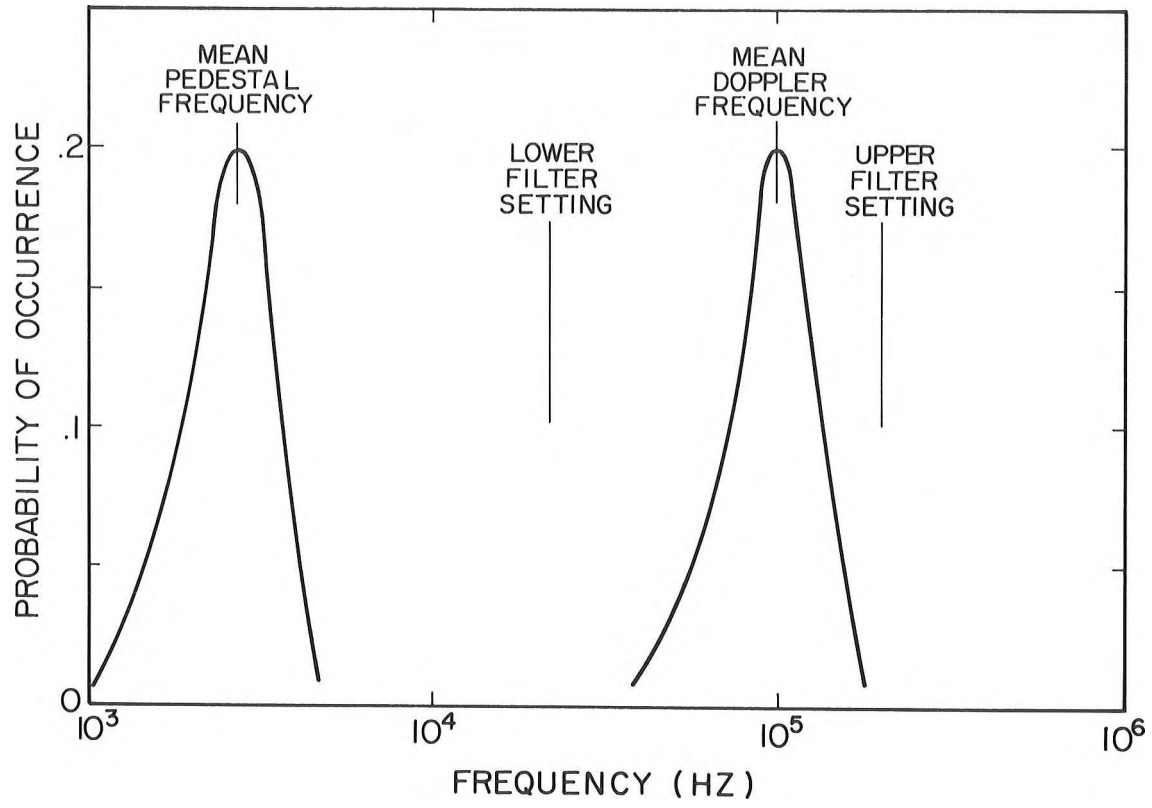

Figure 6. Historgrams of Doppler and Pedestal Frequencies

to electronically filter out the pedestal without also filtering out good Doppler signals. Techniques such as noise cancelling optics (1) can be used to eliminate the pedestal frequency. This is a technique which will eventually be incorporated into this system so that measurements can be made right up to the wall.

The fluid is carefully seeded for each run to yield a dilute concentration of small scattering centers. The entire flow system is carefully cleaned and all make-up water passes through a 1/2 micron filter before entering the flow loop. The fluid is then seeded with a 1 mg/ℓ concentration of 5 to 10 micron diameter particles classified from AC Fine Test Dust which is primarily sand. Using the results of Hjelmfelt and Mockros (6), a 10 micron diameter sand particle should follow a 2500 Hz fluctuation with an amplitude ratio of 0.95. Since most of the turbulent energy in our low speed water flows will be contained in fluctuations with frequencies well below 250 Hz, the seed is adequate for marking the fluid velocities.

It should be noted that the fringe spacing on the anemometer was approximately 5 microns which is approximately the diameter of a typical scattering particle. According to Durst and Whitelaw (4) this should yield efficient "Doppler" signal in comparison with the pedestal signal and indeed this is experimentally the case.

RESULTS

The symmetry of the mean velocity profiles is demonstrated in Figure 7 where measurements from the east side of the channel are compared to measurements from the west side. The Reynolds number based upon a bulk-average velocity and the hydraulic diameter was 24,700. The distance from a wall is "y". The data are compared to the mean velocity profile of Hussain and Reynolds (7) which was measured at a Reynolds number of 35,400. The brackets indicate the 95% confidence interval for the estimate of the mean. As shown by Figure 7, the data indicate that the channel flow is symmetric and that it has the characteristics of a fully developed channel flow.

The two-dimensionality of the channel flow is shown in Figure 8 where centerline velocities are compared at three "z" locations for two Reynolds numbers. The z coordinate is the spanwise coordinate and z = 0 is half way between the top (z = -6 inches) and the bottom (z = +6 inches) of the channel. The center portion of the channel is clearly two-dimensional.

The mean velocity data for four Reynolds numbers are shown in non-dimensional wall layer coordinates in Figure 9. Except for the R_e = 18,500 data set, complete velocity profiles were measured and the wall shear stress, τ_w, was determined by requiring the data for $y^+ > 30$ to fit the expression,

$$U^+ = 5.63 \log_{10} y^+ + 5.0 \qquad (8)$$

Here $U^+ = \bar{U}/u_\tau$ and $y^+ = yu_\tau/\nu$ where $u_\tau = \sqrt{\tau_w/\rho}$. In this and in the remaining figures the data shown for R_e = 24,700 are averages of the east and west wall data. It should also be noted that the R_e = 18,500 data set was essentially a replicate of the near-wall and center-line points of the 17,700 data set. Thus, for the 18,500 data u_τ was estimated from the shear velocity correlation shown later.

There are several important features about the data in Figure 9. First, the number of realization, N, varied from a low of 35 for one center channel point to as many as 250 to 525 for the near-wall region data. These values of N are sufficient so that the 95% confidence intervals for the mean estimates (2) are within 5% of the reported values, for $y^+ \leq 10$ and within 2% for the rest of the data. Obviously, for $y^+ > 30$, the data can be made to fit Equation 8 quite well. More importantly using u_τ determined from the log fit, the corrected data in the near-wall region agrees relatively well with the $U^+ = y^+$ line, particularly in the vicinity of $y^+ = 6$. It is also important to note that the data at R_e = 18,500 was taken some six weeks later than the data at R_e = 17,700 and yet the two sets are reasonably good replicates of one another.

Without the biasing correction, all of the

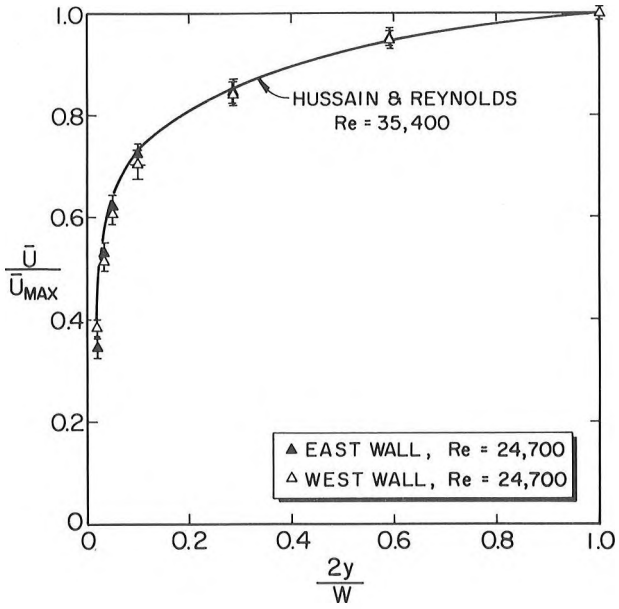

Figure 7. Symmetry Properties of the Turbulent Channel Flow

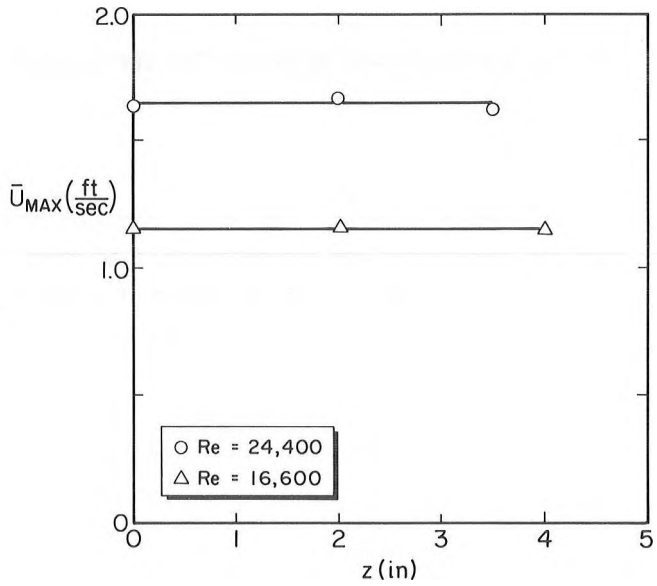

Figure 8. Two-Dimensional Properties of the Turbulent Channel Flow

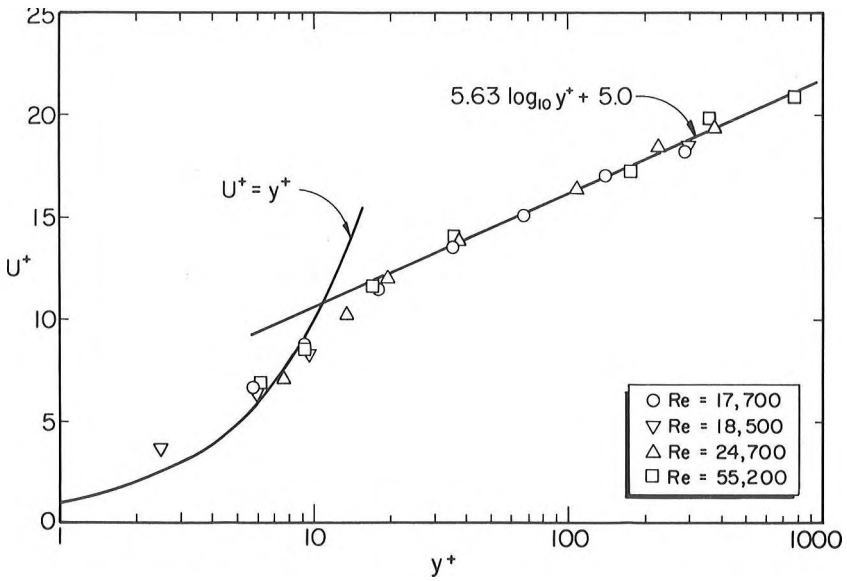

Figure 9. Law of the Wall Mean Velocity Profile

mean velocities for y+ <7 would have fallen above the $U^+ = y^+$ line which is contrary to the high resolution sublayer data of Eckelmann and Reichardt (5). The physical magnitudes of the correction is shown in Figure 10 while the effect in non-dimensional coordinates is shown in Figure 11. The biasing correction has an influence on all of the near-wall data. This correction was a maximum of 13% for the point $y^+ \simeq 3$ and it decreases to insignificant levels as the root mean square of the fluctuation falls below 5% of the local mean velocity.

The data point at $y^+ = 2.5$ is included to demonstrate a practical problem associated with near-wall measurements. For this point, the probe volume center was only 0.0043 in. from the wall. Since the probe volume is approximately 0.0075 inches in diameter, its lower bound extends almost to the wall. Recall that the pedestal frequency component had to be filtered out of the raw Doppler burst signal (as shown in Figure 5). Since the Doppler frequency distribution and the pedestal frequency distribution overlap for this near-wall point, the lower filter setting inevitably filtered a certain amount of the signals scattered from particles on the lower edge of the probe volume, near the wall. Thus the data point at $y^+ = 2.5$, as well as the $R_e = 55{,}200$ point at $y^+ = 6.2$ are biased high.

As mentioned earlier the wall shear stress and wall shear velocity were determined from fitting the data to Equation 8. The wall shear velocity was also estimated from the slope of the velocity profile at the wall by using velocity data from y-locations near $y^+ \approx 6$ and the wall location. Both estimates are compared to data of Hussain and Reynolds (7) on Figure 12. Hussain and Reynold's shear velocities were determined from pressure drop measurements. The agreement between all three determinations is reasonably good. This result is contrary to and supersedes the results and conclusions presented earlier (3).

The root-mean-square estimates of the axial velocity fluctuation are shown in Figure 13. The 95% confidence limits for these estimates, shown by the brackets, were determined using a chi-squared test. They are relatively large because several thousand realizations are required to accurately determine the standard deviation of these histograms. Following the recommendations of McLaughlin and Tiederman (9), no biasing correction has been made to these data. The data are in reasonable agreement with the high resolution data of Eckelmann and Reichardt (5) and Hussain and Reynolds (7) except for the few points nearest the wall where the finite size of the probe volume and the mean velocity gradient cause the measurements to be high. This degree of agreement is quite significant because the ratio of $u'/\overline{U}$ for most of these points was on the order 0.30, and most electronic frequency trackers will not accurately track such large Doppler frequency fluctuations.

DISCUSSION AND CONCLUSIONS

The data clearly indicate that individual realization laser measurements can be successfully made in regions of high turbulent fluctuations. Moreover, when the biasing correction is made to the data, the individual realization estimates of the mean velocity agree well with previous time-average measurements. This confirms our belief that biasing corrections are necessary for individual realization measurements when the velocity fluctuations are large. However, with a biasing correction, accurate estimates can be made in the near-wall region of turbulent flows.

The diameter of the laser probe volume used in this study is an order of magnitude larger than the diameter of a hot-wire probe. However, there is the compensating feature that no physical probe is interfering with the flow. Further, there is the potential for reducing the practical laser anemometer probe volume by a combination of beam expansion and cancellation of the pedestal frequencies (8). Moreover, there are situations where either the sensitivity of the hot wire is low or the calibration is questionable

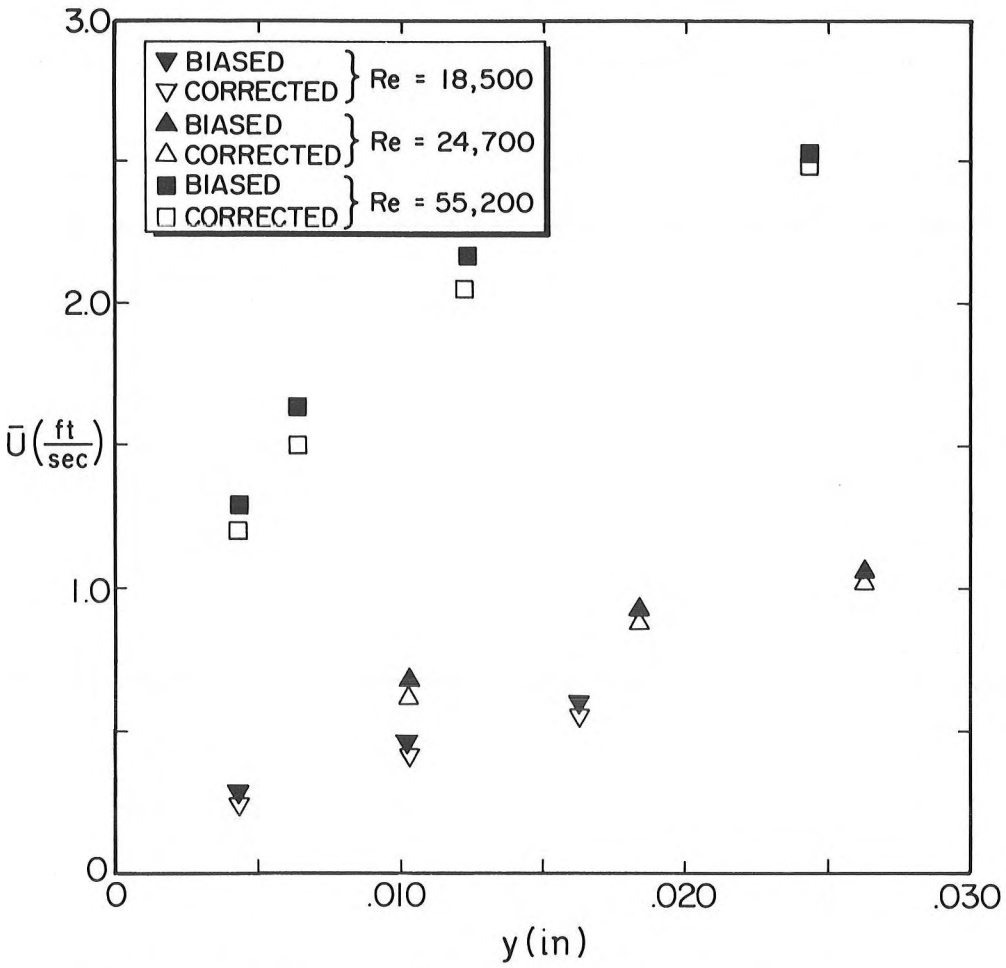

Figure 10. Comparison of Biased and Corrected Mean Velocities in the Near-Wall Region

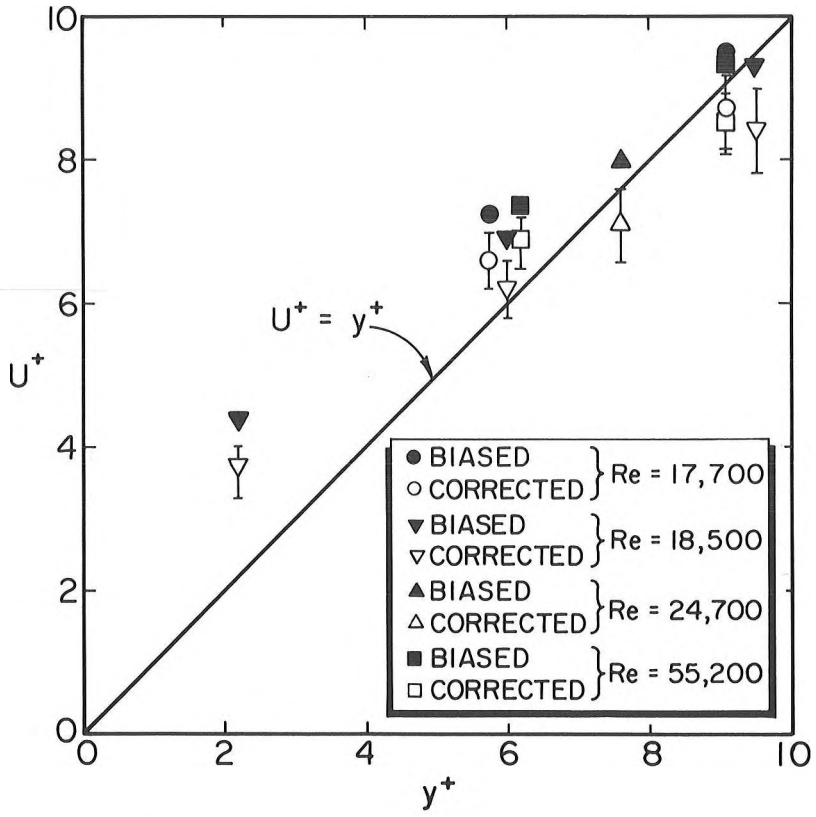

Figure 11. Non-Dimensional Near-Wall Velocity Measurements

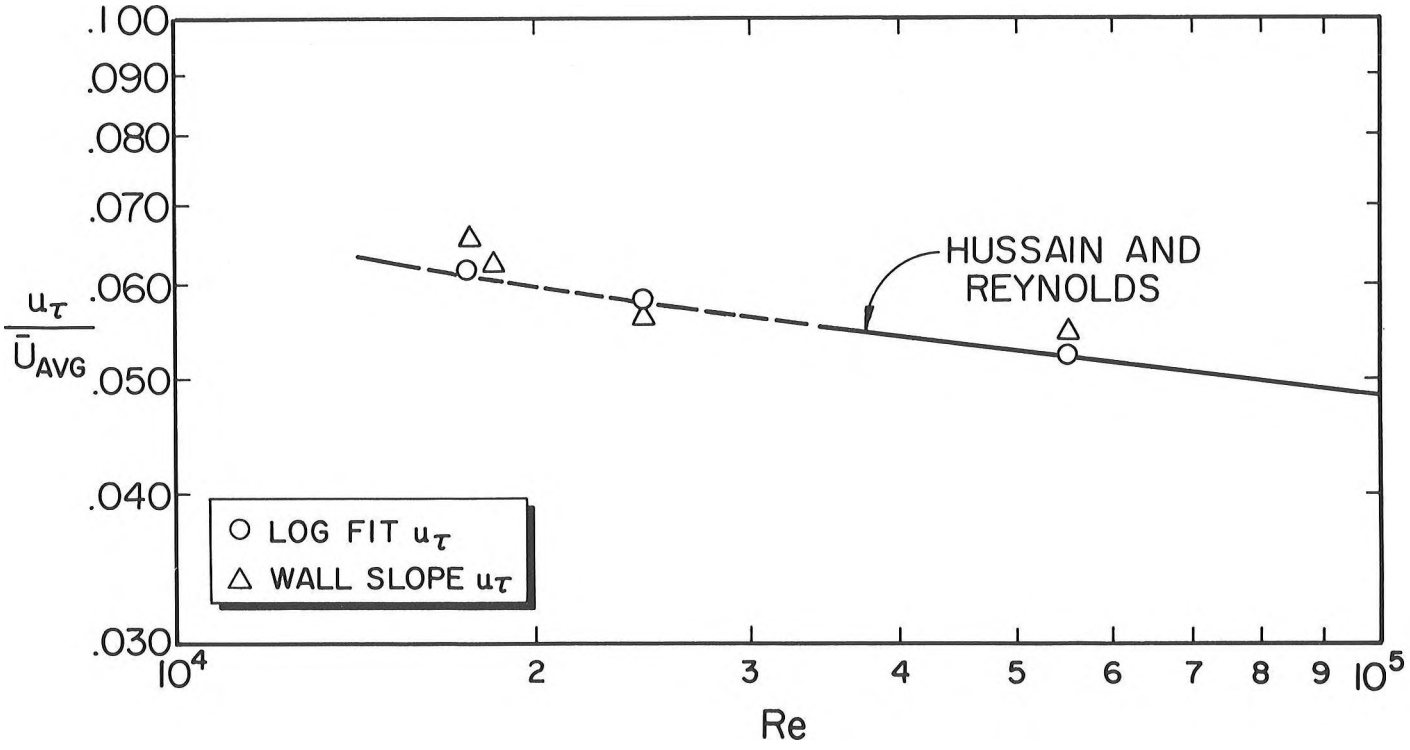

Figure 12. Shear Velocity Correlation

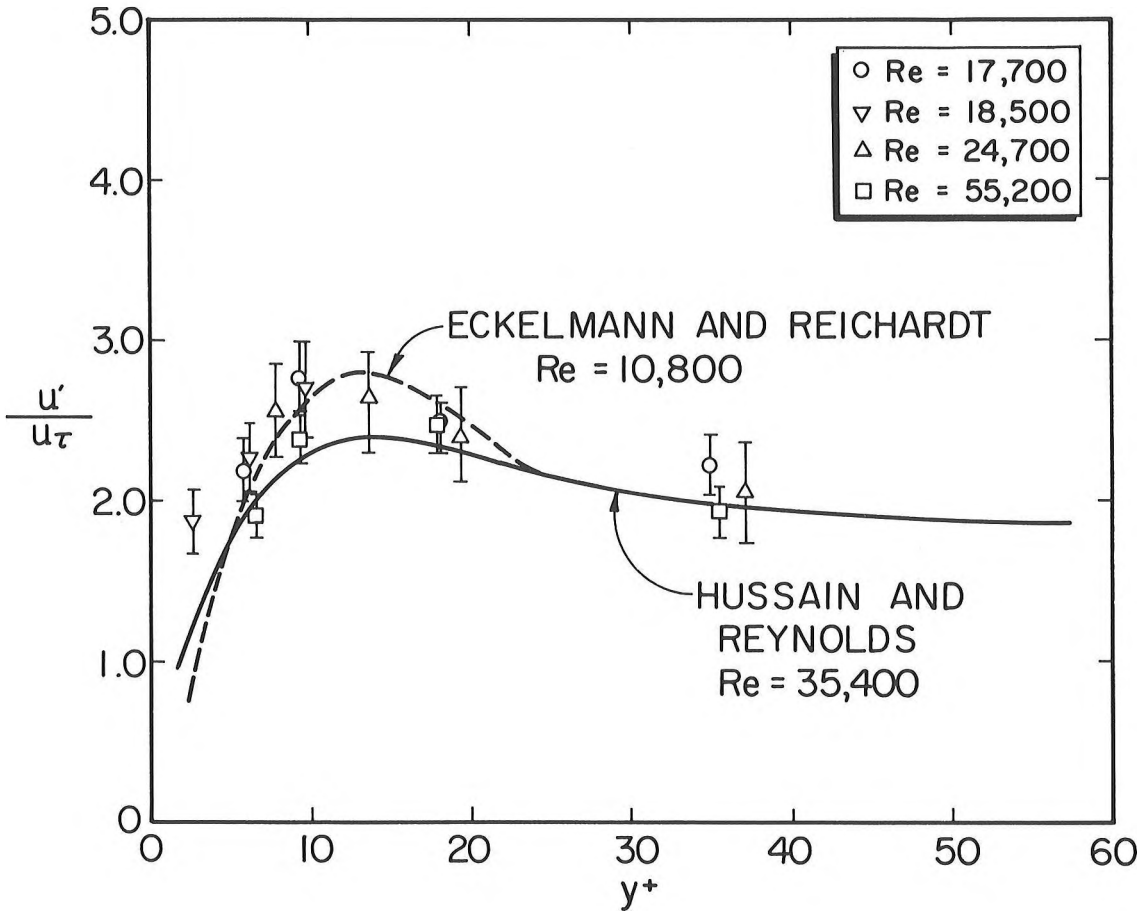

Figure 13. Streamwise Turbulence Intensity Measurements

(such as in dilute polymer, drag-reducing flow). In these cases the individual realization laser anemometer should yield better results despite the larger probe diameter.

SYMBOLS

N	number of individual velocity realizations in a set of data
R_e	Reynolds number
$\overline{T}_D$	average Doppler period for N realizations
t	time
$\overline{U}$	estimate of the mean axial velocity
U^+	non-dimensional axial velocity
$\overline{U}_{avg}$	bulk-average velocity
$\overline{U}_b$	biased estimate of the mean velocity
U_i	individual axial velocity realization
$\overline{U}_{max}$	centerline mean velocity
$\overline{U}_t$	time-average velocity
u'	root mean square of the axial velocity fluctuation
u_τ	shear velocity
$\lvert\overline{V}_i\rvert$	magnitude of an individual realization of the velocity vector
	width of channel
y	distance from the channel wall, normal coordinate
y^+	non-dimensional distance from the wall
z	spanwise coordinate
λ	wave length of the laser light
Θ	angle between the intersecting incident laser beams
ρ	density of fluid
τ_w	wall shear stress
ν	kinematic viscosity of fluid
ω_i	weighting function
γ_i	geometric function of the velocity vector's orientation with respect to the probe volume

REFERENCES

1. Bossel, H. H., Hiller, W. J., and Meier, G.E.A., "Noise-Cancelling Signal Difference Method for Optical Velocity Measurements," J. Physics E., J. Sci. Instr., 5, 893 (1972).

2. Donohue, G. L., McLaughlin, D. K., and Tiederman, W. G., "Turbulence Measurements with a Laser Anemometer Measuring Individual Realizations," Phys. of Fluids, 11, 1920 (1972).

3. Donohue, G. L., Tiederman, W. G. and Reischman, M. M., "Flow Visualization of the Near-Wall Region in a Drag-Reducing Channel Flow," J. Fluid Mech., 56, 559 (1972).

4. Durst, F., and Whitelaw, J. H., "Theoretical Considerations of Significance to the Design of Optical Anemometers," ASME Paper No. 72-HT-7, Presented at the Heat Transfer Conference, Denver, Colorado, 1972.

5. Eckelmann, H., and Reichardt, H., "Hot-Film Measurements in Oil," Proceedings of Symposium on Turbulence in Liquids, Cont. Ed. Series, Univ. of Missouri-Rolla, 1971.

6. Hjelmfelt, A. T., and Mockros, L. F., "Motion of Discrete Particles in a Turbulent Field," Appl. Sci. Res., 16, 149 (1965).

7. Hussain, A. K. M. F., and Reynolds, W. C., "The Mechanics of a Perturbation Wave in Turbulent Shear Flow," Report FM-6, Department of Mechanical Engineering, Stanford University, Stanford, California, 1970.

8. Karpuk, M. E., "A Laser Doppler Anemometer for Viscous Sublayer Measurements," M.S. Thesis, Oklahoma State University, Stillwater, 1974.

9. McLaughlin, D. K. and Tiederman, W. G., " "Biasing Correction for Individual Realization Laser Anemometer Measurements in Turbulent Flows," Phys. of Fluids, 16, 2082 (1973).

DISCUSSION

J. H. Whitelaw, Imperial College: You can, if you want to, make the control volume a great deal smaller. It would require a great deal of mechanical ingenuity. I believe the smallest dimensions I recall are 11 microns from Minneapolis in duct flow - something like that.

Tiederman: Yes, I should have mentioned that we are in the process of constructing beam expanders to reduce our probe volume size. We have a frequency limitation with our data acquisition system and this presents some problems when you reduce the size, however, we believe that we now have a solution for that difficulty.

Whitelaw: I can extend my sympathy to the graduate student, I can see why you didn't do 4000 realizations.

Tiederman: Actually, Mike has now verified as many as 1000 realizations for a limited number of points.

L. L. Lading, Danish Atomic Energy Commission: We've made measurements with a volume of about 15 microns.

P. Iten, Brown Boveri Research Center: I'd like to make a comment on the volume of measurement. This question has arisen many times this morning and I guess it's meaningless to speak solely of the optically given probe volume because the actual probe volume is always strongly dependent on how effective is your electronics and it depends too on the time constant of your electronics. That means that one has to know both. Having a large optical probe volume, as given by the shape of say the surface of where the intensity dropped to 1/e or $1/e^2$, picking up just signals with a high intensity you can electronically decrease the measurement volume.

Tiederman: I would agree in general. In our particular case, we estimate our probe volume size by calculating the fringe spacing and by experimentally determining the maximum number of fringes obtained from our data acquisition system. Most of our signals have essentially the same amplitude because we are scattering off particles that are in a very narrow size range. Based upon this estimate, we obtain an effective probe volume which is certainly dependent upon the seeding and our electronic triggering levels.

Iten: But nevertheless, you get different trajectories with respect to the probe volume even for equal-sized particles and a great variety of different amplitudes. Except in this case by discriminating you can electronically decrease the measurements.

T. J. Hanratty, University of Illinois: I was wondering if you would care to comment on the reliability or the accuracy of Rudd's data in view of the very careful and painstaking effort that you've made in trying to understand all the corrections which are necessary to make turbulence measurements close to the wall.

Reischman: We show some very striking differences between our data and that of Rudd and Logan both. The first is in the mean velocity profile. We don't show the thickening of the viscous sublayer that has been previously presented. The viscous sublayer appears similar for solvent or dilute polymer flows. The main differences in the mean velocity profile appear in the buffer region - that region between the sublayer and the log portion. The second difference between our data and Rudd and Logan is the difference in the turbulent intensities. When normalized with shear velocity, our intensities are lower than previously shown. The peaks of our turbulent intensities are surpressed and less distinct. That is, the maximum values occur over a wider range of Y^+ than previously indicated.

Tiederman: The main conclusion that we've reached is that there is an extended buffer region rather than an extended viscous sublayer in drag reducing flows.